Article

Polyanionic Gallium Hydrides from AlB-Type Precursors AeGaE (Ae = Ca, Sr, Ba; *E* = Si, Ge, Sn)

Michael J. Evans, Gregory P. Holland, Francisco J. Garcia-Garcia, and Ulrich Ha#ussermann

J. Am. Chem. Soc., **2008**, 130 (36), 12139-12147 • DOI: 10.1021/ja803664y • Publication Date (Web): 13 August 2008

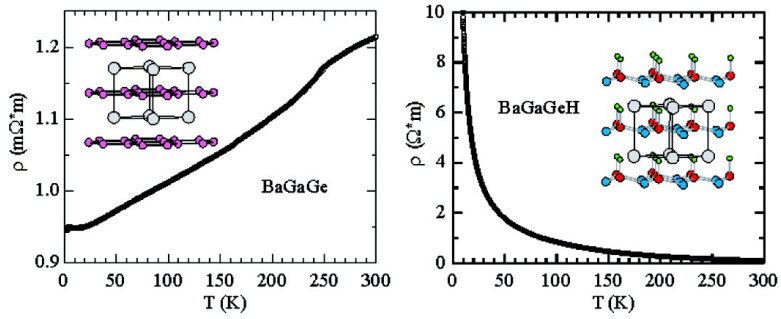

More About This Article

Additional resources and features associated with this article are available within the HTML version:

- Supporting Information
- Access to high resolution figures
- Links to articles and content related to this article
- Copyright permission to reproduce figures and/or text from this article

View the Full Text HTML

J|A|C|S
ARTICLES

Published on Web 08/13/2008

Polyanionic Gallium Hydrides from AlB_2-Type Precursors AeGaE (Ae = Ca, Sr, Ba; *E* = Si, Ge, Sn)

Michael J. Evans,[†] Gregory P. Holland,[†] Francisco J. Garcia-Garcia,[‡] and Ulrich Häussermann*,[†]

Department of Chemistry and Biochemistry, Arizona State University, P.O. Box 871604, Tempe, Arizona 85287-1604, and Lehrstuhl für Festkörperchemie, Institut für Physik, Universität Augsburg, Universitätsstrasse 1, D-86159 Augsburg

Received May 16, 2008; E-mail: Ulrich.Haussermann@asu.edu

Abstract: The quaternary hydrides (deuterides) SrGaGeH(D), BaGaSiH(D), BaGaGeH(D), and BaGaSnH(D) were obtained by investigating the hydrogenation behavior of AeGaE intermetallic compounds (Ae = Ca, Sr, Ba; E = Si, Ge, Sn), and structurally characterized by powder X-ray and neutron diffraction as well as solid state ^{1}H NMR investigations. The new main group metal/semimetal hydrides were found to crystallize with the simple trigonal SrAlSiH structure type (space group *P*3*m*1, *Z* = 1, *a* = 4.22−4.56 Å, *c* = 4.97−5.30 Å) and feature a two-dimensional polyanion $[GaEH]^{2-}$ that corresponds to a corrugated hexagon layer built from three-bonded Ga and E atoms. H is terminally attached to Ga. In BaGaSiD, a considerable degree of stacking disorder could be detected. Polyanions $[GaEH]^{2-}$ are electron precise, and the hydrides AeGaEH display small band gaps in the range of 0.1−0.6 eV at the Fermi level. This is in contrast to the metallic precursor phases AeGaE, which are representatives of the AlB_2 structure type or variants of it. Hydrogenation has only minor consequences for the metal/semimetal atom arrangement, and the induced metal−nonmetal transition is reversible for SrGaGe, BaGaSi, and BaGaGe. BaGaSnH partially decomposes into a mixture of intermetallic compounds upon hydrogen release. Desorption temperatures are above 400 °C.

1. Introduction

Zintl phases, which consist of an active metal (alkali, alkaline earth, or rare earth) and a more electronegative p-block metal or semimetal component (Al, Ga, In, Si, Ge, Sn, etc.), offer a wide range of chemical compositions and crystal structures and have attracted attention for their transport (e.g., thermoelectric clathrates or superconducting silicides) and magnetic properties (e.g., magnetocaloric Gd_5Si_4).[1−7] The peculiarity with Zintl phases is that they are conceptually considered as salts. Electron transfer from the electropositive component leads to reduced p-block atoms, which may polymerize to achieve an octet. Thus, the presence of a covalently bonded polyanionic substructure is a characteristic feature of Zintl phases.

The salt-like concept has stimulated experiments in the chemical reactivity of Zintl phases. Especially noteworthy is the extremely versatile solution chemistry of systems containing deltahedral clusters allowing various functionalization of clusters with organic or organometallic fragments as well as their oxidative coupling into oligomers and polymers,[8] metathesis reactions of systems containing discrete polyhedral anions (e.g., pyramidal $GaTe_3^{3-}$ in K_3GaTe_3) allowing the exchange of the active metal component,[9] and the mild oxidation of alkali metal silicides and germanides into clathrate or zeolite-like frameworks.[10−13] Common to these attempts is the idea to exploit the polyanionic substructure of Zintl phases as a precursor, which can be isolated upon sequestering the cation component, modified in further reactions, or transformed into new metastable p-block arrangements with unique crystal structures.

In this respect, reactions of Zintl phases with gaseous hydrogen also provide interesting possibilities. Earlier work has shown that some electronically imbalanced Zintl phases (e.g., Mn_5Si_3-type $Ca_5Sb_3 = (Ca^{2+})_5(Sb^{3-})_3 \cdot e^-$) incorporate H to yield charge balanced hydrides ($(Ca^{2+})_5(Sb^{3-})_3 \cdot H^-$).[14] In this case, H is exclusively coordinated by s-block metal ions and occurs

[†] Arizona State University.
[‡] Universität Augsburg.

(1) Kauzlarich, S. M., Ed. *Chemistry, Structure and Bonding of Zintl Phases and Ions*; VCH: Weinheim, 1996.
(2) Schäfer, H.; Eisenmann, B.; Müller, W. *Angew. Chem., Int. Ed.* **1973**, *12*, 694–712.
(3) Nesper, R. *Prog. Solid State Chem.* **1990**, *20*, 1–45.
(4) Sevov, S. C. Zintl Phases. In: *Intermetallic Compounds - Principles and Practice (Volume 3)*; Westbrook, J. H., Fleischer, R. L., Eds.; John Wiley & Sons. Ltd.: Chichester, England, 2002; pp 113−132.
(5) Nolas, G. S.; Cohn, J. L.; Slack, G. A.; Schujman, S. B. *Appl. Phys. Lett.* **1998**, *73*, 178–180.
(6) Imai, M.; Nishida, K.; Kimura, T.; Abe, H. *Appl. Phys. Lett.* **2002**, *80*, 1019–1021.
(7) Pecharsky, V. K.; Gschneider, K. A. *J. Alloys Compd.* **1997**, *260*, 98–106.
(8) Sevov, S. C.; Goicoechea, J. M. *Organometallics* **2006**, *25*, 5678–5692, and references therein.
(9) Jung, J.-S.; Wu, B.; Ren, L.; O'Connor, C. J. *J. Appl. Phys.* **1993**, *73*, 5463–5465.
(10) Beekman, M.; Kaduk, J. A.; Huang, Q.; Wong-Ng, W.; Yang, Z.; Wang, D. L.; Nolas, G. S. *Chem. Commun.* **2007**, *8*, 837–839.
(11) Guloy, A. M.; Ramlau, R.; Tang, Z. J.; Schnelle, W.; Baitinger, M.; Grin, Y. *Nature* **2006**, *443*, 320–323.
(12) Ammar, A.; Cros, C.; Pouchard, M.; Jaussaud, N.; Bassat, J. M.; Villeneuve, G.; Reny, E. *J. Phys. IV* **2005**, *123*, 29–34.
(13) Bohme, B.; Guloy, A.; Tang, Z. J.; Schnelle, W.; Burkhardt, U.; Baitinger, M.; Grin, Y. *J. Am. Chem. Soc.* **2007**, *129*, 5348–5349.
(14) Leon-Escamilla, E. A.; Corbett, J. D. *Chem. Mater.* **2006**, *18*, 4782–4792.

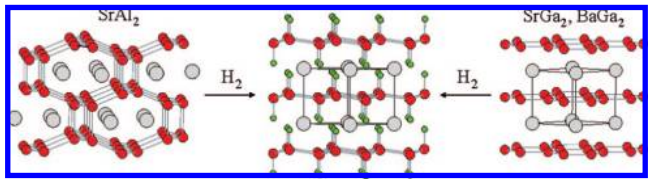

Figure 1. Hydrogenation of $CeCu_2$-type ($SrAl_2$) and AlB_2-type Zintl phases ($SrGa_2$, $BaGa_2$) to $SrAl_2H_2$-type polyanionic hydrides. H, Al/Ga and Sr/Ba atoms are denoted as green, red, and gray circles, respectively.

hydridic, thus acting as an electron sink. Usually the p-block component of imbalanced Zintl phases is not influenced by a hydridic H incorporation. This is different when H reacts with charge balanced Zintl phases as has been recently reported for $CaSi/CaSiH_x$ ($x \approx 1$).[15,16] The incorporation of hydridic H into interstitial sites of the Ca substructure leads to the formation of a new polyanion in response to the reduced electron count for the p-block component.

A conceptually different situation represents the hydrogenation of $CeCu_2$-type $SrAl_2$ where H appears to dissect bonds in the in the precursor polyanion (Figure 1).[17] In $SrAl_2H_2$, hydrogen participates in the polymeric anion where it acts as a covalently bonded terminating ligand to a p-block metal atom. Both precursor and hydride represent electron precise Zintl phases. Interestingly, the $SrAl_2H_2$ structure can also be achieved by hydrogenating the AlB_2-type precursors $SrGa_2$ and $BaGa_2$. In this case, H adds to a formally unsaturated (π-bonded) p-block polyanion (cf. Figure 1). This imposes only very small changes to the structure of the precursor anion.[18]

The formation of $SrAl_2H_2$-type hydrides suggests that the underlying hydrogenation is a true precursor reaction, which preserves the countercation arrangement of the Zintl phase in the hydride. However, mechanisms connected with the incorporation of H in Zintl phases have not yet been investigated. Moreover, it is not generally known which compositions and structures of Zintl phases react with elemental hydrogen, and when hydrogenations lead to interstitial hydrides or to hydrides where H participates in the polyanion (polyanionic hydrides). The hydrogen content of both types of hydrides is comparably low; however, chemical structures and physical properties of Zintl phases can be dramatically influenced by the inclusion of H.

Here, we report a hydrogenation study of a series of 9 isoelectronic compounds AeGaE (Ae = Ca, Sr, Ba; E = Si, Ge, Sn), which crystallize with the simple AlB_2 structure or closely related variants of it. These precursors are not electron precise with respect to the AlB_2 structure (the optimum electron count for a polyanionic graphitic layer is 4 electrons per atom) but display electron excess and are metals. The silicides attracted interest for their superconducting properties,[19−21] for which the partially occupied π^* band plays a decisive role.[22,23] We show that some compositions AeGaE react with hydrogen and form monohydrides AeGaEH where H is terminally bonded to Ga. The incorporation of H induces a very minor rearrangement of the metal atoms. However, the electronic structure is most profoundly affected: Hydrogenation causes a metal-nonmetal transition and turns the electronically imbalanced precursor into an electron precise Zintl phase with a narrow band gap at the Fermi level. This is similar to the earlier reported system SrAlSi/SrAlSiH.[24]

2. Experimental Section

Synthesis. All steps of synthesis and sample preparation for diffraction and thermal analysis experiments were preformed in an Ar-filled glovebox (O_2 concentration < 0.1 ppm). Ca (99.98% purity), Sr (99.95%), Ba (99.9%), Ga (99.999%), and Ge (99.999%) were purchased from Alfa Aesar. Silicon powder and tin shot (both 99.999%) were purchased from Aldrich. The ternary phases AeGaE were prepared by arc-melting stoichiometric mixtures of the pure elements under a high purity Ar atmosphere on a water cooled copper hearth and remelted three times (weight loss was less than 3%). For hydrogenation, the starting materials were pressed into pellets and loaded into corundum crucibles, which were placed into stainless steel autoclaves. Reactions were carried out at 350 °C for 3 days and a hydrogen pressure of 80 bar. The deuterides were prepared analogously, with the exception of BaGaSiD, which required a lower temperature (300 °C) and longer reaction time (4 days). The phase purity of starting materials and hydrides was established by powder X-ray diffraction patterns taken on a Siemens D5000 diffractometer (Bragg−Brentano geometry; Cu Kα radiation; Si standard). The hydrides have a gray color and are, apart from BaGaSnH, relatively air stable.

Structural Characterization. Lattice parameters of the ternary intermetallics SrGaGe and BaGaE, and their hydrides and deuterides were obtained from least-squares refinement of the measured and indexed lines of the corresponding powder diffractograms.[25] Atomic positions of SrGaGeD and BaGaED were determined by Rietveld analysis of neutron powder diffraction data using the programs GSAS and EXPGUI.[26,27] Time-of-flight neutron diffraction data were measured on the neutron powder diffractometer (NPDF) at the Lujan Neutron Scattering Center at Los Alamos National Laboratory. Approximately 3.0 g of each sample were loaded into sealed vanadium canisters and measured at room temperature.

Rietveld Refinement Strategy. For SrGaGeD, BaGaGeD, and BaGaSnD, the refinement strategy was essentially the same. Unit cell parameters were first determined using powder X-ray diffraction with an internal Si standard. Initial values for the atomic coordinates were taken from computationally relaxed structural parameters obtained from first principles calculations. First the unit cell parameters were refined, along with the zero correction. In the early stages of refinement, too much background was being subtracted, so the background was fit graphically and "bootstrapped" until there was better agreement in intensities between the experimental and calculated patterns, especially at low *d*-spacing. Atomic coordinates and U_{iso} were refined to achieve this agreement, then the background was allowed to refine with as few number of terms as possible. At

(15) Aoki, M.; Ohba, N.; Noritake, T.; Towata, S. *Appl. Phys. Lett.* **2004**, *85*, 387–388.
(16) Wu, H.; Zhou, W.; Udovic, T. J.; Rush, J. J.; Yildirim, T. *Phys. Rev. B* **2006**, *74*, 224101.
(17) Gingl, F.; Vogt, T.; Akiba, E. *J. Alloys Compd.* **2000**, *306*, 127–132.
(18) Björling, T.; Noreus, D.; Häussermann, U. *J. Am. Chem. Soc.* **2006**, *128*, 817–824.
(19) Imai, M.; Abe, E.; Ye, J. H.; Nishida, K.; Kimura, T.; Honma, K.; Abe, H.; Kitazawa, H. *Phys. Rev. Lett.* **2001**, *87*, 077003.
(20) Imai, M.; Nishida, K.; Kimura, T.; Kitazawa, H.; Abe, H.; Kito, H.; Yoshii, K. *Phys. C* **2002**, *382*, 361–366.
(21) Imai, M.; Nishida, K.; Kimura, T.; Abe, H. *Phys. C* **2002**, *377*, 96–100.
(22) Shein, I. R.; Medvedeva, N. I.; Ivansivskii, A. L. *J. Phys.: Condens. Matter* **2003**, *15*, L541–L545.
(23) Huang, G. Q.; Liu, M.; Chen, L. F.; Xing, D. Y. *Phys. C* **2005**, *423*, 9–14.
(24) Björling, T.; Noréus, D.; Jansson, K.; Andersson, M.; Leonova, E.; Edén, M.; Hålenius, U.; Häussermann, U. *Angew. Chem., Int. Ed.* **2005**, *44*, 7269–7273.
(25) Werner, P.-E. *Ark. Kemi* **1969**, *31*, 513–516.
(26) Larson, A. C.; Von Dreele, R. B. General Structure Analysis System (GSAS), Los Alamos National Laboratory Report LAUR 86−748, 2004.
(27) Toby, B. H. *J. Appl. Crystallogr.* **2001**, *34*, 210–213.

Table 1. Crystal Data and Structure Refinement of AeGaED[a]

compound	SrGaGeH/D	BaGaSiH/D	BaGaGeH/D	BaGaSnH/D
space group	*P*3*m*1 (No. 156)	*P*3*m*1 (No. 156)	*P*3*m*1 (No. 156)	*P*3*m*1 (No. 156)
Z	1	1	1	1
a, Å	4.2221(4) [4.2278(5)]	4.2776(6) [4.2934(9)]	4.3344(6) [4.3369(5)]	4.559(1) [4.5611(9)]
c, Å	4.9691(6) [4.9673(9)]	5.1948(9) [5.186(1)]	5.1895(9) [5.1931(8)]	5.298(1) [5.309(1)]
c/*a*	1.18	1.21	1.20	1.16
V, Å^3	76.71 [76.89]	82.32 [82.79]	84.43 [84.59]	95.35 [95.67]
temp, K	300	300	300	300
χ^2	2.915	3.610	3.229	2.525
R_p, %	2.49	1.76	2.20	2.39
R_{wp}, %	3.93	2.49	3.31	3.92

[a] Lattice parameters are obtained from X-ray data. Values in brackets refer to AeGaEH.

Table 2. Atomic Coordinates, Isotropic Displacement Parameters (Å^2), and Site Occupancies for AeGaED

atom	Wyckoff position	*x*	*y*	*z*	U_{eq}	*occ.*
			SrGaGeD			
Sr	1*a*	0	0	0	0.0131(2)	1
Ga	1*c*	2/3	1/3	0.5585(2)	0.0200(2)	1
Ge	1*b*	1/3	2/3	0.4402(2)	0.0082(1)	1
D	1*c*	2/3	1/3	0.9056(2)	0.0163(2)	1
			BaGaSiD			
Ba	1*a*	0	0	0	0.0041(3)	1
Ga(1)	1*c*	2/3	1/3	0.5267(8)	0.0163(6)	0.398(6)
Si(1)	1*c*	2/3	1/3	0.5267	0.0163	0.602
D(1)	1*c*	2/3	1/3	0.8403(8)	0.0178(4)	0.398
Ga(2)	1*b*	1/3	2/3	0.4395(10)	0.0257(9)	0.602
Si(2)	1*b*	1/3	2/3	0.4395	0.0257	0.398
D(2)	1*b*	1/3	2/3	0.1071(9)	0.0178	0.602
			BaGaGeD			
Ba	1*a*	0	0	0	0.0084(1)	1
Ga	1*c*	2/3	1/3	0.5432(1)	0.0107(1)	1
Ge	1*b*	1/3	2/3	0.4437(1)	0.0121(1)	1
D	1*c*	2/3	1/3	0.8730(1)	0.0283(2)	1
			BaGaSnD			
Ba	1*a*	0	0	0	0.0126(2)	1
Ga	1*c*	2/3	1/3	0.5509(3)	0.0214(2)	1
Sn	1*b*	1/3	2/3	0.4424(3)	0.0106(2)	1
D	1*c*	2/3	1/3	0.8737(3)	0.0233(3)	1

this stage, secondary phases were added to all three refinements: SrGaGe for SrGaGeD, BaGaGe for BaGaGeD, and a Sn-substituted form of $BaGa_4$ ($BaGa_{4-x}Sn_x$; $x < 0.89$) for BaGaSnD.[28] Next the profile was refined with profile function 4, which employs the result of a convolution between a pair of back-to-back exponentials and a pseudo-Voigt (it should be noted that profile function 1 was first tried, but did not account for the significant Lorentzian contribution to the peak shape). For SrGaGeD and BaGaGeD, the profile for the second phase was also refined, due to overlapping reflections. During profile refinement all other parameters were turned off, with the exception of scale factor, phase fraction for the second phase, and background. Once the profile was adequately modeled, the other parameters were turned on in this order: unit cell, zero point, atomic coordinates, U_{iso}. Finally, the occupancy of D was refined and remained at or very close to 1 (within 0.5%).

For BaGaSiD the same strategy was followed, until the initial refinements of atomic coordinates and U_{iso} were done. At this stage there was poor agreement in intensities between the calculated and experimental patterns for several reflections. A new model was attempted where Ga and Si were randomly distributed on the 1b and 1c sites. A second D position was added at (1/3, 2/3, 0.11). Occupancies were constrained so that the empirical formula BaGaSiD was retained, and each crystallographic site was fully occupied. Atoms on a shared crystallographic site were constrained to have the same U_{iso}, as were the two D positions. A second phase was added to the refinement, in this case $BaGa_4$. The remainder of the refinement strategy was the same as for the other 3 deuterides. Results of the Rietveld refinements are collected in Tables 1 and 2.

Thermal Investigation. The thermal behavior of powdered samples of SrGaGeH, BaGaSiH, BaGaGeH, and BaGaSnH were investigated by differential thermal analysis (Shimadzu DTA-50) and compared with $SrGa_2H_2$ and $BaGa_2H_2$. The latter compounds were prepared according to refs.[18,29] Samples were placed in sealed stainless steel containers to prevent exposure to air and moisture, and the temperature was raised from 30 to 550 °C. The experiments were preformed under a flow of dry Ar and with a temperature increase rate of 5 K/min.

NMR. Solid-state ^{1}H magic angle spinning (MAS) NMR experiments were carried out at room temperature on a Varian VNMRS 400 MHz spectrometer equipped with a 2.5 mm triple resonance MAS probe operating at 399.7 MHz for ^{1}H. Powders of SrGaGeH and BaGaEH were filled in zirconia rotors and spun at a MAS frequency (ω_R) of 25 kHz. The ^{1}H signal transients were recorded with a spin−echo pulse sequence where the $\pi/2$ and π pulse were 3 and 6 μs, respectively. The τ delay between pulses and following the second pulse was set to one rotor period and a recycle delay of 60 s was utilized. The ^{1}H chemical shift was referenced indirectly by setting the ^{1}H resonance of adamantane to 1.63 ppm.

(28) Tobash, P. H.; Yamasaki, Y.; Bobev, S. *Acta Crystallogr., E* **2007**, *63*, i35−i37.

(29) Lee, M. H.; Evans, M. J.; Daemen, L. L.; Sankey, O. F.; Häussermann, U. *Inorg. Chem.* **2008**, *47*, 1496–1501.

TEM. Samples for transmission electron microscopy were prepared under dry argon. The powders were ground in a mortar and the fine resulting crystallites were supported onto holey-carbon coated copper grids. Transfer of the sample into the sample holder and into the electron microscope was done under normal air conditions. In the electron microscope, the samples were always crystalline and no indication of a reaction with oxygen and/or moisture was observed. Specimens were studied in a JEOL JEM 2000FX and JEOL JEM 2100F. The latter is equipped with an EDAX detector for X-ray energy-dispersive spectrometry.

Property Measurements. The electrical resistivity of BaGaGe and BaGaGeH was measured on a Quantum Design PPMS system equipped with an AC transport controller (Model 7100), with a current of 100 μA and a frequency of 16 Hz using a four point in-line contact arrangement. The BaGaGe sample was prepared by arc-melting and shaped to a bar with dimensions 2.0 × 2.0 × 1.4 mm. The BaGaGeH sample was obtained by hydrogenating BaGaGe. Subsequently the brittle sample was compacted into a cylinder with dimensions 2.0 × 2.2 × 1.5 mm by employing 5 GPa in a multianvil high pressure apparatus. This afforded a cold pressed sample with a density corresponding to the theoretical one. The integrity of the hydride after high pressure treatment was confirmed by powder X-ray diffraction. Contacts were painted on the sample using a two-component silver epoxy (Epo-Tek H20E) and cured at 150 °C for 5 min. Copper or gold wires were used to connect the contacts to the sample holder using an air drying silver paint (Demetron D200). Resistivity was measured during both heating and cooling in the interval 2−350 K with a rate of 0.5 K/min. Temperature-dependent magnetization of BaGaGe was measured by the Vibrating Sample Magnetometer (VSM) on the PPMS system. The arc-melted sample was placed in a brass trough sample holder with a small amount of fast-curing superglue and loaded vertically into the chamber. The temperature was scanned from 10 to 2 K at a rate of 0.1 K/min.

Electronic Structure Calculations. Total energy calculations for AeGaE and AeGaEH (Ae = Ca, Sr, Ba; E = Si, Ge, Sn) were performed in the framework of the frozen core all-electron Projected Augmented Wave (PAW) method,[30] as implemented in the program VASP.[31] The energy cutoff was set to 500 eV. Exchange and correlation effects were treated by the generalized gradient approximation (GGA), usually referred to as PW91.[32] The integration over the Brillouin zone was done on special k-points determined according to the Monkhorst-Pack scheme.[33] Total energies were converged to at least 1 meV/atom. Structural parameters were relaxed until forces had converged to less than 0.01 eV/Å. For AeGaE the ordered AlB_2 structure (SrPtSb-type, SG: $P\bar{6}m2$), the ordered $EuGe_2$ structure (SG: $P3m1$) and the YPtAs structure (SG: $P6_3/mmc$) were considered. For AeGaEH only the SrAlSiH structure was taken into account. The computationally obtained structural parameters for AeGaE and AeGaEH are given as Supporting Information.

3. Results

Precursor Phases AeGaE. The systems AeGaE provide a unique compositional playground; all 9 possible combinations can be prepared from arc melting stoichiometric mixtures of the elements. Previously known were CaGaGe, CaGaSn, SrGaGe, SrGaSn, and BaGaGe, which crystallize with the hexagonal YPtAs-type (space group $P6_3/mmc$), and CaGaSi, SrGaSi, and BaGaSi with the hexagonal AlB_2-type ($P6/mmm$).[20,34]

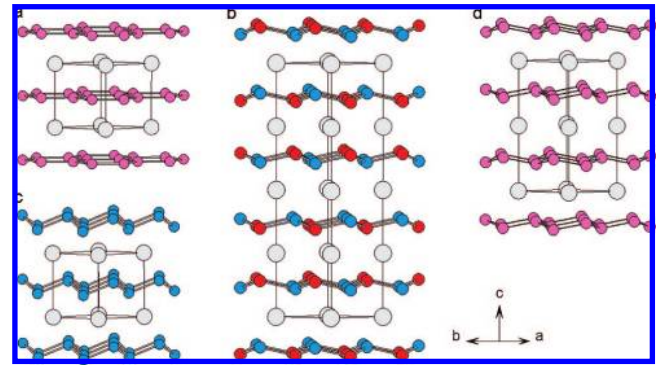

Figure 2. Crystal structures of (a) AlB_2, (b) YPtAs, (c) $EuGe_2$, and (d) $CaIn_2$.

The latter systems are most likely part of extended solid solutions $AeGa_{2-x}Si_x$ ($\approx 0.6 < x < \approx 1.3$).[21] Our synthesis attempts also afforded BaGaSn, which according to powder X-ray diffraction crystallizes with the AlB_2 type structure. Compared to the other samples, CaGaSn displayed a poorer crystallinity and could not be obtained as a single phase product. Interestingly, by arc-melting, SrGaGe and BaGaGe were obtained with a different crystal structure compared to the previously reported one.[34] Powder X-ray diffraction patterns showed clearly the presence of the AlB_2 structure for both systems (and not the YPtAs type).

The AlB_2 and YPtAs structure are closely related (Figure 2).[35] In the simple AlB_2 type Ga and E atoms are randomly distributed over the site of the majority atoms forming planar hexagon layers (Figure 2a). If Ga and E atoms are completely ordered in a way that each atom is coordinated by three unlike ones, the AlB_2-type unit cell is maintained but space group symmetry is reduced from $P6/mmm$ to $P\bar{6}m2$. This results in the SrPtSb structure. Usually 9-electron AlB_2-type systems, which also include the AeAlSi and various REAlE/REGaE (RE = divalent rare earth metal) compositions,[36] are assumed to display different degrees of order. This depends on the preparation method and especially preparation temperature.[37] For CaAlSi, specially synthesized single crystals even displayed the completely Al/Si ordered SrPtSb structure.[38]

The YPtAs structure can be regarded as a ternary derivative of the AlB_2 type structure where puckering of the hexagon layers produces a 4-fold superstructure along the c direction (Figure 2b). The puckered hexagon layers are now formed by atoms on two different crystallographic sites. As in the AlB_2 structure, the hexagon layers are stacked on top of each other; however, the orientation of layers and distribution of atoms produces an arrangement of double layers where Ga and E atoms are located at the inside and outside, respectively.[35] Recently You et al. presented a detailed investigation of the EuGaE systems where EuGaSi adopts the AlB_2 type and the heavier homologues the YPtAs type.[39] This is the same structural trend as for CaGaE and SrGaE.[34] However, our results show that the size of the electropositive component should have a large influence on

(30) (a) Blöchl, P. E. *Phys. Rev. B* **1994**, *50*, 17953. (b) Kresse, G.; Joubert, J. *Phys. Rev. B* **1999**, *59*, 1758.
(31) (a) Kresse, G.; Hafner, J. *Phys. Rev. B* **1993**, *47*, 558. (b) Kresse, G.; Furthmüller, J. *Phys. Rev. B* **1996**, *54*, 11169.
(32) Perdew, J. P.; Wang, Y. *Phys. Rev. B* **1992**, *45*, 13244.
(33) Monkhorst, H. J.; Pack, J. D. *Phys. Rev. B* **1976**, *13*, 5188.
(34) Czybulka, A.; Pinger, B.; Schuster, H.-U. *Z. Anorg. Allg. Chem.* **1989**, *579*, 151–157.
(35) Hoffmann, R.-D.; Pöttgen, R. *Z. Kristallogr.* **2001**, *216*, 127–145.
(36) Villars, P. Calvert, L. D. *Pearsons Handbook of Crystallographic Data for Intermetallic Compounds*, 2nd ed.; ASM International: Materials Park, OH, 1997.
(37) Lue, C. S.; Xie, B. X.; Fang, C. P. *Phys. Rev. B* **2006**, *74*, 014505.
(38) Kuroiwa, S.; Sagayama, H.; Kakiuchi, T.; Sawa, H.; Noda, Y.; Akimitsu, J. *Phys. Rev. B* **2006**, *74*, 014517.
(39) You, T. S.; Grin, Y.; Miller, G. J. *Inorg. Chem.* **2007**, *46*, 8801–8811.

Table 3. Structural Parameters for AlB_2 Precursor Zintl Phases

compound	SrGaGe[a]	BaGaSi	BaGaGe	BaGaSn[a]
a, Å	4.275(1)	4.247(1)	4.3352(4)	4.5800(7)
c, Å	4.703(2)	5.109(1)	5.0928(5)	5.1638(9)
c/*a*	1.10	1.20	1.18	1.13
d_{Ga-E}, Å	2.468(1)	2.452(1)	2.503(1)	2.644(1)
V, Å^3	74.48	79.83	82.89	93.81

[a] Superstructure.

structural competition. A larger size favors the formation of the AlB_2 type: SrGaGe is probably polymorphic and can also be obtained with the AlB_2 structure. Further, the YPtAs structure is not found in the series of BaGaE systems. The simplest puckered variant of the AlB_2-type is the trigonal $EuGe_2$ structure (Figure 2c) where the layers are formed from one kind of atoms, oriented the same way, and stacked on top of each other along the *c* direction (space group $P\bar{3}m1$).[35] Note that the degree of puckering as expressed in the torsion angle is lower in YPtAs-type CaGaGe and SrGaSn, around 43 and 55°, respectively, compared to $EuGe_2$ (67°).[34,40]

Table 3 compiles the structural parameters of AlB_2 type SrGaGe and BaGaE as obtained from powder X-ray diffraction. Going from SrGaGe to BaGaGe naturally increases significantly the *c* lattice parameter, but also *a*. The Ga−Ge distance within the hexagon layers increase from 2.47 to 2.50 Å. The *c*/*a* ratio increases from 1.1 to 1.18. Within the series BaGaE, the *a* parameter increases from 4.25 to 4.58 Å when going from E = Si to Sn, while the *c* parameter varies (increases) just slightly. The *c*/*a* ratio decreases from 1.2 to 1.13. The presence of the AlB_2 structure for BaGaSi and BaGaGe was unambiguously confirmed by TEM investigations (Figure 3a). However, for SrGaGe and BaGaSn selected area electron diffraction revealed weak superstructure reflections. In the case of SrGaGe, they correspond to a commensurate 5-fold superstructure along the hexagonal *c* direction (Figure 3b). A similar phenomenon was reported for samples of CaAlSi and found to correspond to modulated corrugations of the hexagon layers.[41] These corrugations, however, are very weak compared to the pronounced puckering in the YPtAs structure, and the superstructure reflections are not observable with X-ray powder diffraction. In the case of BaGaSn, superstructure reflections corresponded to a doubling of the AlB_2 *c* axis (Figure 3c). This is compatible with two types of puckered hexagon layers that are mutually rotated by 60° (stacked in antiphase orientation). The arrangement is isopointal to ordered NdPtSb or ScAuSi.[35] However, reflection conditions indicate space group $P6_3/mmc$, which implies randomly disordered Ga and Sn. Thus, BaGaSn should be considered as isostructural to $CaIn_2$ with weakly puckered hexagon layers (Figure 2d).

Hydrogenation Reactions. The prepared phases AeGaE were exposed to a hydrogen (deuterium) atmosphere of 80 bar at 350 °C. With these conditions, four of them yielded isostructural monohydrides: SrGaGeH, BaGaSiH, BaGaGeH, and BaGaSnH. SrGaSn reacted with hydrogen, but the product(s) could not be characterized at this stage. Especially, it is not clear if a ternary hydride different from the others was formed or if the hydrogenation induced a decomposition into X-ray amorphous SrH_2 and a new ternary intermetallic Sr−Ga−Sn compound. It

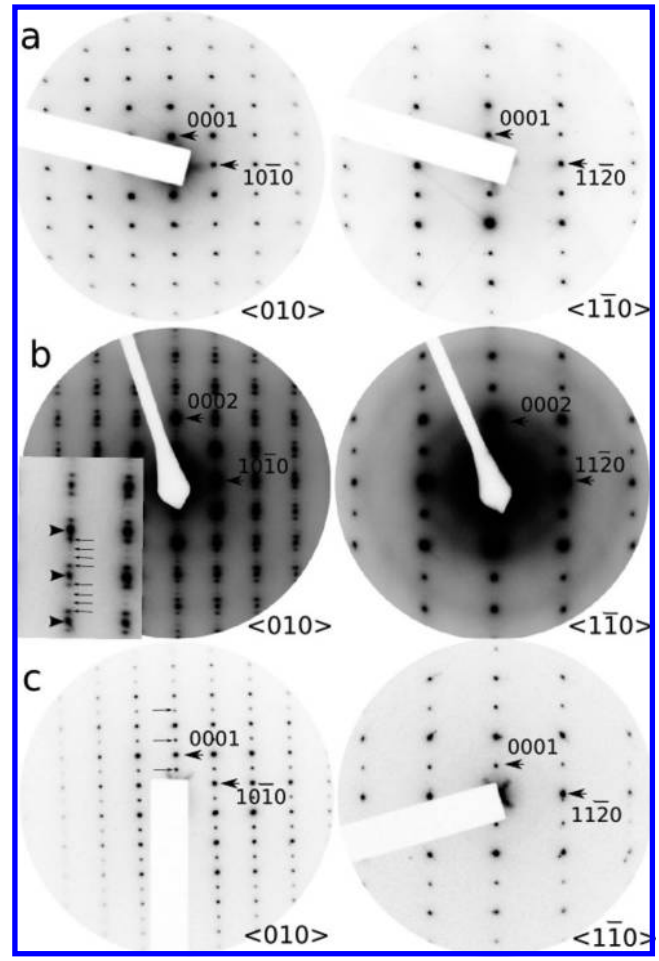

Figure 3. Zone axis electron diffraction patterns down ⟨010⟩ (left-hand panel) and ⟨1$\bar{1}$0⟩ (right-hand panel) of (a) BaGaSi, (b) SrGaGe, and (c) BaGaSn. The BaGaSi crystals show the typical reciprocal lattice for the AlB_2 structure type, while SrGaGe and BaGaSn crystals show different superstructure ordering along *c**. The inset in (b) is a magnified section of the SrGaGe ⟨010⟩ diffraction pattern to emphasize the emerging 5-fold superstructure. Reflections belonging to the parent AlB_2 structure type are indicated with arrowhead, satellite reflections with arrows.

is interesting to note that the monohydrides are all based on AlB_2-type precursors, or modulated variants of it. The other four compounds (CaGaE and SrGaSi) remained unchanged upon hydrogenation. Subsequently, hydrogenation experiments on SrGaGe and BaGaE were performed at lower and higher temperatures (150−600 °C). Hydride formation was not observed after 24 h unless a reaction temperature of at least 275 °C was applied. Further, temperatures above 425 °C did not yield hydrides but rather led to decomposition of the precursor, which was especially apparent with BaGaSn. When applying the initial hydrogenation conditions for reacting SrGaGe and BaGaE with deuterium, BaGaSi remained unchanged, and the reaction temperature had to be lowered to 300 °C for obtaining BaGaSiD.

Crystal Structure of SrGaGeD and BaGaED (E = Si, Ge, Sn). The structures of SrGaGeD and BaGaED were established from the Rietveld refinement of neutron diffraction powder data. All four compounds are isostructural to already reported SrAlSiH (Figure 4a and Tables 1 and 2).[24] The trigonal structure of the AeGaED compounds (space group $P3m1$) displays slightly puckered hexagon layers in which Ga and E atoms are arranged strictly alternating. These layers are stacked on top of

(40) Bobev, S.; Bauer, E. D.; Thompson, J. D.; Sarrao, J. L.; Miller, G. J.; Eck, B.; Dronskowski, R. J. *Solid State Chem.* **2004**, *177*, 3545–3552.
(41) Sparta, K. M.; Müller, R.; Merz, M.; Roth, G.; Adelmann, P.; Wolf, T. *Acta Crystallogr. B* **2006**, *62*, 710–718.

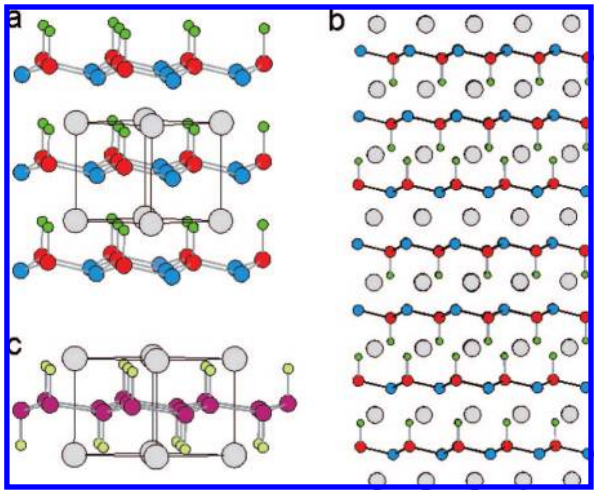

Figure 4. (a) Crystal structure of SrAlSiH-type AeGaED. (Ae, Ga, E, and H atoms are depicted as gray, red, blue, and green circles, respectively). (b) Sketch of the "random flip" disorder model of BaGaSiD and (c) refined average structure. (Purple circles indicate mixed occupied Ga/Si positions, and light green circles indicate partially occupied D positions).

Table 4. Selected Interatomic Distances (Å) and Angles (deg) in AeGaED

		SrGaGeD	BaGaSiD	BaGaGeD	BaGaSnD
Ae−D	3×	2.482	2.606(1)/ 2.532(1)	2.587(0)	2.713(0)
Ae−Ga	3×	3.279(1)	3.363(4)	3.446(0)	3.544(1)
Ae−E	3×	3.275(1)	3.485(3)	3.399(1)	3.521(1)
Ga−D	1×	1.725(2)	1.629(6)/ 1.726(7)	1.711(1)	1.708(3)
Ga−E	3×	2.507	2.512(1)	2.554(0)	2.691(1)
Ga−E−Ga		114.68(4)	117.1(1)	116.02(2)	115.58(5)
E−Ga−D		103.56(4)	99.9(1)	101.66(3)	102.32(6)
torsion		44.20(5)	33.17(18)	38.59(3)	40.56(7)

each other with the same orientation and sandwich Ae atoms. Thus, the metal arrangement corresponds to that of the $EuGe_2$ structure (cf. Figure 2c). Interatomic distances and angles in AeGaED are given in Table 4.

D is exclusively attached to Ga and further coordinated by three Ae atoms. The Ga−D distance in the deuterides is around 1.71 Å and does not appear to be susceptible to the different chemical environments. Although the Ga−D distance in AeGaED formally corresponds to that of a terminal bond, it is relatively long compared to terminal Ga−H bond lengths in molecular species GaH_n (n = 1, 2, 3)[42−45] or in the tetrahedral complex GaH_4^- occurring in $NaGaH_4$.[46,47] However, it is similar to the Ga−H distance in the isoelectronic dihydrides $SrGa_2H_2$ and $BaGa_2H_2$ (cf. Figure 1) with the $SrAl_2H_2$ structure (1.69 Å).[18,29]

Overall, the different compositions AeGaED produce only slight variations within the SrAlSiH structure. The torsion angle (i.e., degree of puckering) decreases from 44 to 39° when going from SrGaGeD to BaGaGeD and increases from 33 to 41° when going from E = Si to Sn within the BaGaE series. This correlates inversely with the *c/a* ratio. The degree of puckering in SrAlSiH-type systems AeGaED is smaller than in isoelectronic $EuGe_2$ with the $EuGe_2$ structure (67°)[40] but larger than in $SrGa_2H_2$ and $BaGa_2H_2$ with the $SrAl_2H_2$ structure (<30°).[18] In the SrAlSiH structure, Ae is only coordinated by three H atoms. This is the most conspicuous difference to the $SrAl_2H_2$ structure where Ae atoms are surrounded by 6 H atoms. The Ae−D distance in the SrAlSiH representatives AeGaED is shorter than in $SrGa_2D_2$ and $BaGa_2D_2$ (2.48 vs 2.59 Å for Ae = Sr and around 2.60 vs 2.68 Å for Ae = Ba), apart for BaGaSnD where the Ba−D distance (2.71 Å) is slightly larger than in $BaGa_2D_2$. The Ga−D distance is somewhat larger in AeGaED than in $AeGa_2D_2$ (around 1.71 vs 1.69 Å). Both type of system possess electron precise polyanions, $[(GaH)E]^{2-}$ and $[(GaH)(GaH)]^{2-}$, with structures in accord with the Zintl concept.

A structural peculiarity was encountered with BaGaSiD. The initial refinements of the SrAlSiH-type model yielded poor agreement between calculated and measured intensities and structural disorder was suspected. This disorder could then be best described by a random "layer flip" where a flipped and an original puckered hexagon layer are related by a center of inversion (Figure 4b). As a consequence, the average structure resembles that of $SrAl_2H_2$,[18] but with two different Al and H positions. The two Al atoms correspond to a mixture of 60% Ga and 40% Si, and vice versa. Accordingly, with D exclusively bonded to Ga atoms, the D positions are 60% and 40% occupied, respectively. In the refined disordered model, the lower occupied D position is closer to Ga ($d_{Ga1\text{-}D1}$ = 1.63 Å)—and accordingly further away from Ba—than the higher occupied one ($d_{Ga2\text{-}D2}$ = 1.73 Å). This may coincide with the trend that the Ga−D distance in dihydrides $AeGa_2D_2$ is longer than in monohydrides AeGaED (by 0.02 Å) but appears exaggerated. The disorder feature was only observed for BaGaSiD and may be connected to the lower reaction temperature that had to be applied for obtaining this compound. A TEM electron diffraction investigation of BaGaSiH(D) did not reveal further information in terms of superstructure reflections or diffuse streaking along the *c** direction. However, TEM studies of BaGaSiH(D) may not be conclusive because of the possibility that H(D) desorbs under the electron beam, which is impossible to detect because of the small structural difference to the precursor BaGaSi.

NMR Investigations. Figure 5 shows magic-angle spinning (MAS) ^{1}H NMR spectra from powders of SrGaGeH and BaGaEH. Each spectrum is characteristic of a single site, with a shoulder. For the BaGaEH series, the ^{1}H chemical shift is 4.0−4.5 ppm with the shoulder positioned at around 2.5 ppm. The chemical shift is noticeably different for the SrGaGeH sample where the primary site has a chemical shift of 6.2 ppm (shoulder at around 4.5 ppm). Clearly, the type of Ae atom has a higher impact on the observed ^{1}H chemical shift than the E component surrounding the Ga atom to which H is attached. A two-dimensional (2D) double quantum/single quantum (DQ/SQ) NMR correlation spectrum was collected for the BaGaGeH sample (see Supporting Information). This 2D spectrum shows an off-diagonal correlation between the two sites, which indicates that the two sites are spatially close (<5 Å). Therefore, the shoulder is not the result of an impurity phase but, rather that two proton sites are present in the same material. The observation of two sites for BaGaSiH can be explained by the stacking disorder as identified for BaGaSiD from neutron diffraction. However, the presence of two hydrogen sites for remaining compounds is surprising. One possibility is that

(42) Aldridge, S.; Downs, A. J. *Chem. Rev.* **2001**, *101*, 3305.
(43) Ito, F.; Nakanaga, T.; Takeo, H.; Jones, H. *J. Mol. Spectrosc.* **1994**, *164*, 379.
(44) Pullumbi, P.; Mijoule, C.; Manceron, L.; Bouteiller, Y. J. *Chem. Phys.* **1994**, *185*, 13.
(45) Pullumbi, P.; Bouteiller, Y.; Manceron, L.; Mijoule, C. *Chem. Phys.* **1994**, *185*, 25.
(46) Iniguez, J.; Yildirim, T.; Udovic, T. J.; Sulic, M.; Jensen, C. M. *Phys. Rev. B* **2004**, *70*, 060101.
(47) Irodova, A. V.; Somenkov, V. A.; Bakum, Si. I.; Kuznetsova, S. F. *Z. Phys. Chem. Neue Fol.* **1989**, *163*, 239.

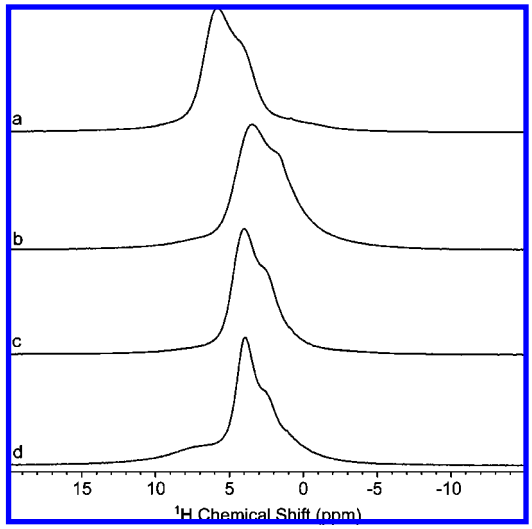

Figure 5. ^{1}H MAS NMR spectrum of (a) SrGaGeH, (b) BaGaSiH, (c) BaGaGeH, and (d) BaGaSnH.

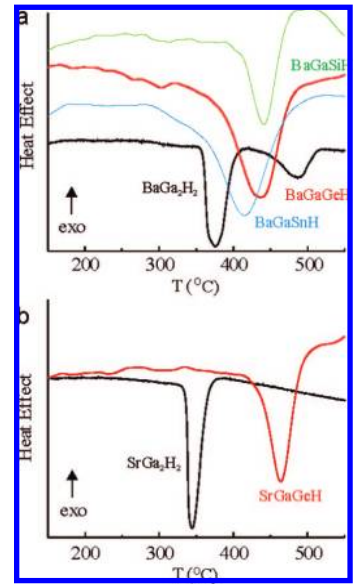

Figure 6. DTA heating curves for (a) $BaGa_2H_2$ and BaGaEH (E = Si, Ge,Sn) and (b) $SrGa_2H_2$ and SrGaGeH.

hydrides investigated by NMR and deuterides investigated by neutron diffraction behave slightly different in terms of structural disorder. ^{2}H NMR experiments are not conclusive because lower resolution of the ^{2}H spectrum does not allow detection of the shoulder feature.

To determine if the shoulder feature was the result of the disordered structure present in BaGaSiD (see Figure 4), DQ spinning sideband patterns were collected to measure the H−H dipolar coupling and extract the internuclear distance. Both the primary and shoulder component of the ^{1}H resonance displayed identical spinning sideband patterns. The H−H dipolar coupling was extracted from simulations of the DQ spinning sideband pattern (see Supporting Information). A value of 1700 Hz was obtained, which corresponds to a 4.2 Å distance. This distance is consistent with the primary structure and provides no evidence to support the disordered structure where a significantly closer approach of 2.8 Å is expected. This indicates that the disordered structure is unique to BaGaSiD and is not present to any large extent in the protonated samples. Thus, the origin of the shoulder peak in the ^{1}H NMR spectra of SrGaGeH and BaGaEH remains unclear.

Thermal Stability. Figure 6 shows the DTA heating curves for the monohydrides SrGaGeH and BaGaEH, and for the dihydrides $SrGa_2H_2$ and $BaGa_2H_2$ under isochoric conditions at atmospheric pressure (inert gas). For SrGaGeH, a sharp endothermic event is observed that starts around 420 °C corresponding to the loss of hydrogen; this event occurs at about 330 °C for $SrGa_2H_2$. Decomposition begins at lower temperatures for BaGaEH. For BaGaGeH and BaGaSnH, the endothermic event seems to start around 300−350 °C, although the bulk of hydrogen desorption happens beyond 400 °C. Once again, decomposition occurs at lower temperatures for the dihydride ($BaGa_2H_2$) compared to the monohydrides. For SrGaGeH, BaGaSiH, and BaGaGeH, the AlB_2-type precursor phases were regained after desorption, while for BaGaSnH a partial decomposition into ternary intermetallic phases occurred of which $BaGa_{4-x}Sn_x$ could be identified.

4. Discussion

The 9-electron systems AeGaE represent charge imbalanced (not electron precise) Zintl phases. The electronic structure of a planar hexagon layer formed by main group atoms is characterized by three bonding σ bands. Additionally the Ga and E-p_z orbitals give rise to two π bands, one bonding and one antibonding. Due to the different energies of Ga and E-p_z orbitals the bonding π band has a larger E-p_z contribution, and vice versa, the antibonding π^* band has a larger Ga-p_z contribution. As a consequence, the topology and dispersion of the π bands is rather different compared to (electron precise) 8-electron systems where the hexagon layers are formed by one kind of atom (e.g., $SrGa_2$ and $BaGa_2$). For the 9-electron systems AeGaE, the Ga-p_z based π^*-band becomes partially occupied. Additionally, one Ae-d band with mainly d_{z2} character crosses the Fermi level and systems AeGaE are metals.[22,23]

Puckering of hexagon layers destroys the π bands and creates more localized (lone pair) electronic states. For example, the simple $EuGe_2$ structure contains arsenic-like polyanionic layers and is electron precise for 10 electrons per formula unit. Thus, with respect to a puckered layer derivative of the AlB_2-type, the 9-electron systems AeGaE are electron deficient. Interestingly, although electron balanced, $EuGe_2$ remains a metallic conductor. Similar to AlB_2 type AeGaE systems, Eu-d bands cross the Fermi level.[40]

The electronic imbalance of 9-electron systems bears interesting consequences. AlB_2-type AeGaSi and AeAlSi have been shown to display superconducting properties.[6,19−21,48] The origin of these properties lies in the partially occupied π^* and Ae-d states in conjunction with a peculiar soft phonon mode associated with the out-of-plane vibration of the hexagon layer.[49−51] This is rather different compared to the famous isostructural

(48) Lorenz, B.; Lenzi, J.; Cmaidalka, J.; Meng, R. L.; Sun, Y. Y.; Xue, Y. Y.; Chu, C. W. *Phys. C* **2002**, *383*, 191–196.
(49) Mazin, I. I.; Papaconstantopoulos, D. A. *Phys. Rev. B* **2004**, *69*, 180512.
(50) Huang, G. Q.; Chen, L. F.; Liu, M.; Xing, D. Y. *Phys. Rev. B* **2004**, *69*, 064509.
(51) Giantomassi, M.; Boeri, L.; Bachelet, G. B. *Phys. Rev. B* **2005**, *72*, 224512.

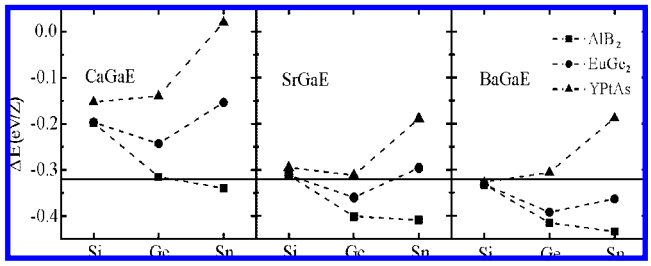

Figure 7. Computed zero-temperature formation energy for the reaction AeGaE + $1/2H_2$ = AeGaEH. For AeGaE, three different structure types were considered. The horizontal line represents the value for ΔG of half a molecule of H_2 at 550 K.

8-electron system MgB_2[52] where partially occupied σ bonding states couple strongly to in-plane vibrations of boron.[53]

The formation of the four monohydrides SrGaGeH and BaGaEH from corresponding precursor AeGaE proceeds with only minor structural changes. Considering the precursors either in the disordered AlB_2 structure (*P6/mmm*) or in the ordered, noncentrosymmetric, SrPtSb structure ($P\bar{6}m2$), hydrogenation causes the loss of hexagonal symmetry due to the puckering of Ga−E layers and in AeGaEH space group symmetry is reduced to *P3m*1 (Figure 1a). The symmetry reduction from the AlB_2 to the SrAlSiH structure can be simply expressed as two consecutive translationengleiche steps of index two (t2) where ordering implies the loss of the inversion center and puckering the loss of the horizontal mirror plane.[35] Hydrogen incorporation is accompanied with a peculiar small volume increase of about 2 Å^3. Naturally, the *c* lattice parameter is most affected and expands upon puckering of hexagon layers, whereas the *a* parameter varies only slightly. The Ga−E distance of the hexagon layer increases by about 0.05 Å for all systems.

Why are monohydrides only obtained from SrGaGe and BaGaE? We addressed this question by calculating zero-temperature formation energies for the reaction AeGaE + 1/2 H_2 → AeGaEH for all nine compositional combinations and considering AeGaE in three different structures, SrPtSb (ordered AlB_2), ordered $EuGe_2$ (space group *P*3m1), and YPtAs. The result is displayed in Figure 7. The first interesting observation is that these 9-electron systems only prefer the planar structure for E = Si, whereas germanides and especially stannides have a strong tendency toward puckering. (Thus in Figure 7 the $EuGe_2$ and YPtAs structures display a lower formation energy with respect to the hydrogenation reaction). This is in agreement with the observation of You et al. for EuGaE[39] and the earlier reported structures for CaGaE and SrGaGe.[34] It is then surprising that our arc-melting synthesis did not afford SrGaGe and BaGaSn with the YPtAs structure but modulated AlB_2 structures, which indicates a randomly disordered Ga/E distribution. Polymorphism of these systems correlating to the thermal history of samples seems then to be plausible.

Hydrogenations reactions involve a gaseous species, and thus, hydride formation is entropically disfavored. The temperature-dependent Gibbs free energy ($\Delta G_{(T)}H_2$) for a H_2 gas molecule with respect to the temperature of 0 K is around −0.67 eV at 550 K,[54] which is about the activation temperature that has to be applied for transforming AeGaE into monohydrides. Subtracting half of this value from the formation energies in Figure 7 gives an estimate of the Gibbs free energy of the hydrogenation reaction which reflects well the experimental findings:[55] (a) Monohydrides never form for the CaGaSi, CaGaGe, and SrGaSi systems; (b) Monohydrides never form if the precursor adopts the ordered YPtAs structure with puckered layers (CaGaSn, SrGaSn); (c) For BaGaSi, hydride formation is close to zero Gibbs free energy, which may correlate with the observed structural disorder in BaGaSiD.

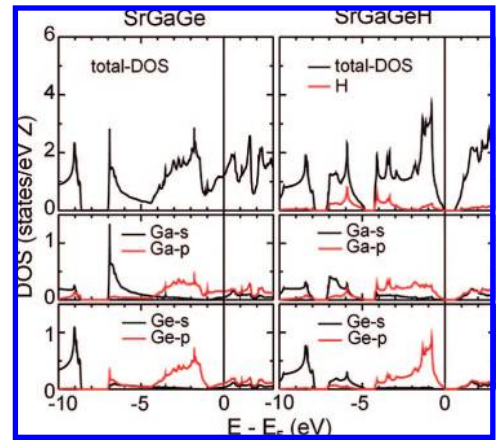

Figure 8. Electronic density of states (DOS) and orbital decomposed DOS for SrGaGe (left panel) and SrGaGeH (right panel). Vertical lines indicate the Fermi level.

Although hydrogen incorporation induces only small changes in the metal/semimetal atom arrangement, the transition from 9-electron precursors AeGaE to electron precise 10-electron hydrides AeGaEH is accompanied with drastic changes in the electronic structure. This is shown representatively in the DOS for SrGaGe/SrGaGeH as depicted in Figure 8. The DOS for all hydrides AeGaGeH is given in the Supporting Information. As already mentioned, 9-electron systems are metals with a partly occupied antibonding π^* band and Ae-d bands crossing the Fermi level. The lowest lying σ band is essentially composed of E-s orbitals and energetically detached from the other two occupied σ bands.[22,23] The larger Ga-p_z orbital contribution to the π^* band is apparent in the higher p-DOS contribution for Ga compared to Ge around the Fermi level. Hydrogen incorporation in AeGaE removes the partly occupied antibonding π^* band and transforms it into an energetically low lying Ga−H bonding band. In turn, the fully occupied bonding π band changes to a weakly dispersed band with E-p_z (lone pair) character in the hydride, which becomes located just below the Fermi level. Its dispersion is about 1, 1.5, and 2 eV for Ae = Ba, Sr, Ca systems, respectively.

The polyanionic hydrides AeGaEH are electron precise with a real band gap at the Fermi level. These band gaps are of indirect nature (similar to earlier investigated SrAlSiH),[24] and the computational values vary between 0.1 (BaGaGeH and BaGaSnH) and 0.6 eV (disorder-free BaGaSiH). According to the Zintl concept, the layered polyanion $[GaEH]^{2-}$ consists of three-bonded $[Ga-H]^-$ and three-bonded, lone pair carrying E^- entities. The charge of the polyanion is counterbalanced by Ae^{2+} cations. This view is justified by the low contribution of Ae states to the occupied bands in AeGaEH.

The hydrogen induced metal−nonmetal transition is also clearly seen in property changes and demonstrated here with

(52) Nagamatsu, J.; Nakagawa, N.; Muranaka, T.; Zenitani, Y.; Akimitsu, J. *Nature* **2001**, *410*, 63–64.
(53) Choi, H. J.; Roundy, D.; Sun, H.; Cohen, M. L.; Louie, S. G. *Nature* **2002**, *418*, 758–760.
(54) Ke, X.; Tanaka, I. *Phys. Rev. B* **2005**, *71*, 024117.

(55) This estimate neglects zero point energies, the effect of pressure, and the temperature dependence of the internal energy.

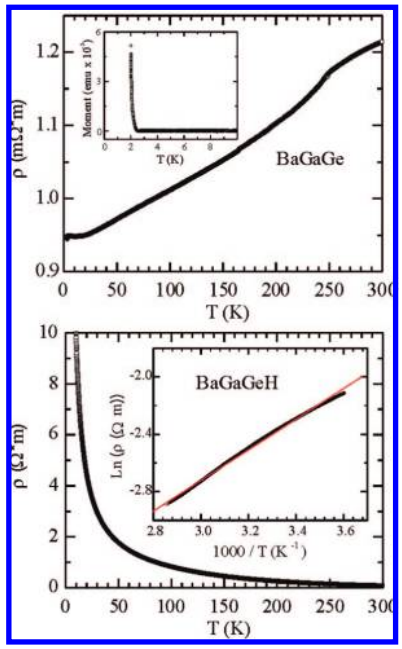

Figure 9. Resistivity of BaGaGe (upper panel) and BaGaGeH (lower panel) as a function of temperature. The inset in the upper panel displays the magnetic moment of BaGaGe between 2 and 10 K. The inset in the lower panel is an Arrhenius plot of the resistivity of BaGaGeH between 300 and 350 K.

the electrical resistivity for BaGaGe/BaGaGeH (Figure 9). BaGaGe has a metallic resistivity behavior and is a superconductor with a T_c of just above 2 K. In the resistivity measurement, the lowest temperature was just above the critical temperature, but superconductivity in BaGaGe was clearly apparent in a subsequently performed temperature-dependent magnetization experiment. This is an important result showing that superconductivity in 9-electron AlB_2-type systems is not restricted to silicides.[56] However, whereas BaGaSi has a T_c of 4.1 K,[20] that of BaGaGe is considerably lower.

The resistivity of BaGaGeH demonstrates clearly a semiconducting behavior. The room temperature value is about 0.1 Ωm. Resistivity values from 300 to 350 K (highest measured temperature) show approximately an Arrhenius temperature dependency, indicating intrinsic resistivity. The band gap estimated from the Arrhenius plot is about 0.1 eV, which actually is in good agreement with the calculated value. The NMR results also support the semiconducting nature of these materials where rather long (>10 s) ^{1}H spin−lattice (T_1) relaxaion times and no appreciable Knight shift were observed. Short (<1 s) T_1 relaxation times and a Knight shift would be expected if these materials were metallic.

Hydrogen induced metal−nonmetal transitions are usually accompanied with a major reconstruction of the metal atom arrangement because the nonmetallic state implies the presence of covalently bonded or hydridic hydrogen.[57] However, this is different in the systems AeGaE/AeGaEH, where metal and hydride structures are connected by group−subgroup relations and the overall bonding situation of metal/semimetal atoms is maintained upon hydrogen incorporation.

5. Conclusions

The reaction of Zintl phases with gaseous hydrogen offers the possibility to alter polyanionic structures and thus physical properties. We show that the metallic Zintl phases SrGaGe and BaGaE (E = Si, Ge, Sn)—which are, in the case of BaGaSi and BaGaGe, superconductors—can be hydrogenated to semiconducting polyanionic hydrides SrGaGeH and BaGaEH. The structure of the hydrides corresponds to that of SrAlSiH-type whereas the metallic phases adopt the AlB_2 structure (BaGaSi, BaGaGe) or modulated variants of it (SrGaGe, BaGaSn). Although multinary hydride formation from Zintl phase precursors is not well investigated, two scenarios may be discerned: (1) Incorporated hydrogen appears hydridic and exclusively coordinated by active metal ions. Then H acts as an electron sink and reduces the electron count for the p-block component. This is the case for CaSi/$CaSiH_x$ and most likely for Ca_2Si/Ca_2SiH_x ($x \approx 2.41$) where hydrogenation of Co_2Si type precursor with formally completely reduced Si atoms (Si^{4-}) leads to an amorphous product with probably polyanionic Si moieties.[58] (2) H participates in the polyanion as formally neutral, terminating, ligand to a p-block atom (polyanionic hydrides). This is the case for $SrAl_2$/$SrAl_2H_2$, $AeGa_2$/$AeGa_2H_2$, SrAlSi/SrAlSiH, and the here reported systems AeGaE/AeGaEH. Both scenarios provide new coordination environments and bonding situations for the atoms involved, which is interesting from a fundamental point of view but also bears opportunities for material properties.[59]

Acknowledgment. This research has been supported by National Science Foundation grant DMR-0638826 and has made use of the Manuel Lujan, Jr. Neutron Scattering Center at Los Alamos National Laboratory, which is funded by the Department of Energy's Office of Basic Energy Sciences. Los Alamos National Laboratory is operated by Los Alamos National Security, LLC, under DOE Contract DE-AC52-06NA25396. We are grateful to Yang Wu and Thomas Proffen for assistance in the property measurements and neutron powder diffraction data collection, respectively. G.P.H. acknowledges support from DOE through grant DE-FG02-05ER46235 and the ASU Magnetic Resonance Research Center.

Supporting Information Available: S1: Rietveld fits to the neutron powder diffraction patterns of SrGaGeD, BaGaSiD, BaGaGeD, and BaGaSnD. S2: DOS curves for all nine AeGaEH systems. S3: Table of computationally relaxed structural parameters for AeGaEH. S4: Two-dimensional double quantum/single quantum (DQ/SQ) NMR correlation spectra for BaGaGeH together with a description of this experiment. S5: DQ spinning sideband pattern for BaGaSiH and simulations to extract H−H distance. This material is available free of charge via the Internet at http://pubs.acs.org.

JA803664Y

(56) Meng, R. L.; Lorenz, B.; Cmaidalka, J.; Wang, Y. S.; Sun, Y. Y.; Lenzi, J.; Meen, J. K.; Xue, Y. Y.; Chu, C. W. *IEEE T Appl. Supercon.* **2003**, *13*, 3042–3046.
(57) Yvon, K.; Renaudin, G.; Wei, C. M.; Chou, M. Y. *Phys. Rev. Lett.* **2005**, *94*, 066403.
(58) Wu, H.; Zhou, W.; Udovic, T. J.; Rush, J. J. *Chem. Mater.* **2007**, *19*, 329–334.
(59) Lee, M. H.; Sankey, O. F.; Björling, T.; Moser, D.; Noréus, D.; Parker, S. F.; Häussermann, U. *Inorg. Chem.* **2007**, *46*, 6987–6991.